



**HAL**  
open science

## CCR2-Dependent Recruitment of Tregs and Monocytes Following Radiotherapy Is Associated with TNF $\alpha$ -Mediated Resistance

Michele Mondini, Pierre-Louis Loyher, Pauline Hamon, Marine Gerbé de Thoré, Marie Laviron, Kevin Berthelot, Céline Clemenson, Benoît Salomon, Christophe Combadière, Eric Deutsch, et al.

### ► To cite this version:

Michele Mondini, Pierre-Louis Loyher, Pauline Hamon, Marine Gerbé de Thoré, Marie Laviron, et al.. CCR2-Dependent Recruitment of Tregs and Monocytes Following Radiotherapy Is Associated with TNF $\alpha$ -Mediated Resistance. *Cancer Immunology Research*, 2019, 7 (3), pp.376-387. 10.1158/2326-6066.CIR-18-0633 . hal-02339936

**HAL Id: hal-02339936**

<https://hal.sorbonne-universite.fr/hal-02339936v1>

Submitted on 30 Oct 2019

**HAL** is a multi-disciplinary open access archive for the deposit and dissemination of scientific research documents, whether they are published or not. The documents may come from teaching and research institutions in France or abroad, or from public or private research centers.

L'archive ouverte pluridisciplinaire **HAL**, est destinée au dépôt et à la diffusion de documents scientifiques de niveau recherche, publiés ou non, émanant des établissements d'enseignement et de recherche français ou étrangers, des laboratoires publics ou privés.

## **CCR2 dependent recruitment of Tregs and monocytes following radiotherapy is associated with TNF $\alpha$ -mediated resistance**

Michele Mondini<sup>1,2,3\*</sup>, Pierre-Louis Loyher<sup>4\*</sup>, Pauline Hamon<sup>1,2,3,4</sup>, Marine Gerbé de Thoré<sup>1,2,3</sup>, Marie Laviron<sup>4</sup>, Kevin Berthelot<sup>1,2,3</sup>, Céline Clémenson<sup>1,2,3</sup>, Benoit L. Salomon<sup>4</sup>, Christophe Combadière<sup>4</sup>, Eric Deutsch<sup>1,2,3,5#</sup>, Alexandre Boissonnas<sup>4#</sup>

<sup>1</sup> Gustave Roussy, Université Paris-Saclay, SIRIC SOCRATE, F-94805, Villejuif, France

<sup>2</sup> INSERM, U1030, Labex LERMIT, F-94805, Villejuif, France

<sup>3</sup> Univ Paris Sud, Université Paris-Saclay, F-94270, Le Kremlin-Bicêtre, France

<sup>4</sup> Sorbonne Université, Inserm, CNRS, Centre d'Immunologie et des Maladies Infectieuses Cimi-Paris, F-75013, Paris, France

<sup>5</sup> Gustave Roussy, Université Paris-Saclay, Département de Radiothérapie, DHU TORINO, F-94805, Villejuif, France

\* Contributed equally

# Share senior authorship

**Running title:** Tregs/monocytes crosstalk dampens radiotherapy efficacy

**Keywords:** radiotherapy, monocytes, regulatory T cells, chemokines, TNF $\alpha$

**Financial support:** P.L.L. was funded by the "Fondation ARC pour la Recherche sur le Cancer". P.H. was funded by the "Ligue contre le cancer". K.B. was funded by "Fondation pour la Recherche Médicale" and "Fondation ARC pour la Recherche sur le Cancer". This work was supported by funding from the European Community's Seventh Framework Programme (FP7/2007-2013) n°304810 – RAIDs (to A.B., E.D. and M.M.), Inserm, "Fondation ARC pour la recherche sur le cancer" (Projets Fondation ARC to M.M. and A.B.) and the "Ligue contre le cancer" (to A.B.).

### **Correspondence to:**

Alexandre Boissonnas

CIMI U1135, 91 Bd de l'hôpital, 75013 Paris, France

Tel. +33140779840 ; E-mail: alexandre.boissonnas@upmc.fr

Michele Mondini

Gustave Roussy, Inserm U1030, 114 rue Edouard Vaillant, 94805 Villejuif, France

Tel. +33142114282 ; E-mail: michele.mondini@gustaveroussy.fr

**Competing interests:** The authors declare no potential conflicts of interest.

**Word count:** 4693; **Figures:** 6

## **ABSTRACT**

Radiation therapy (RT) represents one of the main anticancer approaches for the treatment of solid tumors. Beyond the expected direct effects of RT on tumor cells, evidence supporting the importance of an immune response to radiotherapy is growing. The balance between RT-mediated immunogenic and tolerogenic activity is ill-defined and deserves more attention. Herein, a murine model of head and neck squamous cell carcinoma (HNSCC) was used to demonstrate that RT strongly upregulated CCL2 chemokine production in tumor cells, leading to a CCR2-dependent accumulation of tumor necrosis factor alpha (TNF $\alpha$ )-producing monocytes and CCR2<sup>+</sup> regulatory T cells (Tregs). This co-recruitment was associated with the TNF $\alpha$ -dependent activation of Tregs, dampening the efficacy of RT. Our results highlight an unexpected crosstalk between innate and adaptive immune system components and indicate CCL2/CCR2 and TNF $\alpha$  as potential clinical candidates to counterbalance the radioprotective action of monocyte-derived cells and Tregs, paving the way for potent combined radioimmunotherapies.

## INTRODUCTION

Radiation therapy (RT) is a widely employed anticancer treatment and serves as a mainstay for the management of head and neck squamous cell carcinoma (HNSCC) (1). The effects of RT on the priming and effector phases of antitumor immunity makes it an appealing strategy to generate immunity against the patient's own tumor (2) and an interesting combinational tool to improve several anticancer immunotherapies (3, 4). While radiation is known to enhance the infiltration of activated T cells in the tumor microenvironment (TME) (5, 6), local immunosuppression in the TME is most frequently maintained or even amplified by RT. Regulatory T cells (Tregs) and tumor-associated macrophages (TAMs) represent the main protagonists shaping the immunosuppressive TME and promoting tumor growth, and experimental evidence in murine models has demonstrated that the absence of either of Tregs or TAMs mostly delay tumor progression (7, 8). Macrophage and Treg infiltration into tumors is associated with poor prognosis, therapeutic failure and tumor relapse in multiple solid cancers (9). The chemokine-chemokine receptor network plays key roles in shaping the TME into an immunosuppressive site by inducing the differential recruitment of regulatory and effector immune cells (10). For instance, the CCL2/CCR2 axis represents a major marker of tumor development and has predictive value following cancer therapy in both human and mouse models (11). Recent studies have demonstrated that RT-induced CCL2 production by the tumor contributes to therapeutic failure (12-14), but the mechanisms involved remain elusive. The CCR2-dependent recruitment of Ly6C<sup>high</sup> monocytes can substantially contribute to the TAM compartment (15, 16). Recently, we showed that CCR2 mediates the recruitment of a subset of CCR2<sup>+</sup> Tregs in different tumor models as well as in human oral squamous cell carcinoma (OSCC) (17). We thus hypothesized that the CCL2/CCR2 axis might be implicated in the co-recruitment of TAMs and Tregs following RT and the constitution of TME immunosuppression. The action of Tregs on innate monocyte-derived cells *in vivo* has been poorly investigated thus far. Here, we showed that performing local RT on oral tumors in mice induced a CCR2-dependent accumulation of Tregs and TNF $\alpha$ -producing monocytes and macrophages in the tumor bed. Tregs interacted with monocytes/macrophages in irradiated tumors and, finally, TNF $\alpha$  inhibition reduced Treg activity and was associated with increased RT efficacy.

## MATERIAL AND METHODS

### Cells and animal models

Firefly luciferase-expressing TC1/Luc cells, generated by the HPV16 E6/E7 and c-H-ras retroviral transduction of lung epithelial cells of C57BL/6 origin, were kindly provided by T.C. Wu (Johns Hopkins Medical Institutions, Baltimore, MD, USA) in 2009. Expression of E6 and E7 genes was confirmed by RT-PCR, as well as MHC haplotype H2b by flow cytometry (18). The TdTomato TC1 cell line was generated by infection of TC1 cells with a tdTomato lentivirus

(kindly provided by Dr. N. Bercovici and M. Lambert, Institut Cochin, Paris, France). Master stocks of the cells were prepared upon receipt and then used within 6 months after resuscitation. The cells were injected at submucosal sites on the right inner lips of mice to establish a head and neck tumor implantation model as previously described (18). The RAW 264.7 monocyte/macrophage cell line was obtained from ATCC (Manassas, VA, USA).

C57BL/6 mice were purchased from Janvier CERT (Le Genest St. Isle, France) and housed at the Gustave Roussy animal facility (Plateforme d'Evaluation Preclinique, PFEP) and the Centre d'exploration fonctionnelle, Pitié-Salpêtrière (Paris France). C57BL/6-Foxp3<sup>tm1Mal</sup> mice (called Foxp3-EGFP mice herein) (19), *Ccr2*<sup>-/-</sup> mice, and *Csf1r*-Gal4VP16/UAS-ECFP (MacBlue) (20) mice were intercrossed to generate Foxp3-EGFP x MacBlue, Foxp3-EGFP x MacBlue x *Ccr2*<sup>-/-</sup> mice. These strains, *Foxp3*<sup>tm3(DTR/GFP)Ayr</sup> (Foxp3-DTR) (21) and MMTV-PyMT-P2A-mCherry-P2A-OVA (PyMT-ChOVA) (22), were bred at the Centre d'Exploration Fonctionnelle, Pitié-Salpêtrière (Paris, France). All animal procedures were performed in accordance to protocols approved by the Ethical Committee CEEA 26 and CEEA 05 and validated by the "Service Protection et Santé Animales, Environnement".

### **Irradiation**

Mice received single-beam local irradiation to the head and neck region 7 days after tumor inoculation using a 200 kV Varian X-ray irradiator. Selective irradiation of the tumor grafts was performed by the interposition of a 4-cm-thick lead shield on a schedule delivering 7.5Gy in a single fraction at a dose rate of 1.08Gy/min.

### **Antibodies and treatments**

The anti-CD25 (*InVivo*MAb anti-mouse CD25, clone PC-61.5.3) and anti-TNF $\alpha$  (*InVivo*MAb anti-mouse TNF $\alpha$ , clone XT3.11) neutralizing antibodies as well as the corresponding isotype controls (*InVivo*MAb rat IgG1 isotype control, anti-horseradish peroxidase, clone HRPN) were purchased from BioXcell (West Lebanon, NH, USA). Anti-CD25 was administered at 20 mg/kg in PBS by intraperitoneal (IP) injection on days 4 and 6 post-RT. Anti-TNF $\alpha$  was administered at 25 mg/kg in PBS by IP injection on days 2 and 4 post-RT. To deplete Tregs in Foxp3-DTR mice, diphtheria toxin (DTx, Merck, USA) was solubilized in PBS and injected IP at 1  $\mu$ g/mouse on days 2 and 3 post-RT. DTx treatment had no effects on tumor growth in WT mice (not shown).

### ***In vivo* imaging**

To monitor tumor growth, bioluminescence imaging was performed using the Xenogen *In Vivo* Imaging System 50 (IVIS; Caliper Life Sciences, Hopkinton, MA, USA) as previously described (18).

For multiphoton imaging of Foxp3-EGFP x MacBlue mice, HNSCC tumors were carefully collected and immobilized in an imaging chamber perfused with oxygenated (95% O<sub>2</sub> plus 5% CO<sub>2</sub>) RPMI medium containing 10% fetal calf serum (FCS). The local temperature was monitored and maintained at 37°C. The two-photon laser scanning microscopy setup used

was previously described (20), and the excitation wavelength used was 870 nm. The system included a set of external nondescanned detectors in reflection with a combination of LP-600 nm followed by LP-462 nm and LP-500 nm dichroic mirrors to split the light and collect the second-harmonic generation (SHG) signal with a 417/60 nm emission filter, ECFP with a 480/40 nm emission filter and EGFP with a 525/50 nm emission filter.

Cell motility was measured every 30 s by 9 consecutive 5  $\mu\text{m}$  z spacing stacks (total of 40  $\mu\text{m}$  thickness) using a plan apochromat 20 $\times$  (NA=1) water immersion objective. Fluorescent cells were monitored over time with 3-dimensional automatic tracking and manual correction with Imaris software (Bitplane, Zurich, Switzerland). The acquisition and analysis protocols for all experimental conditions to be compared were identical. Velocity and straightness were determined using Imaris. The track straightness corresponded to the ratio of the distance between the initial and final positions of each cell to the total distance covered by the same cell.

### **Histological analysis**

Tumors were harvested, fixed in 4% formalin for 4 h, incubated in 30% sucrose-PBS overnight at 4°C, embedded in Tissue-Tek OCT compound (Sakura Finetek, Alphen aan den Rijn, Netherlands) and frozen at -80°C. Sectioning was completed on an HM550 cryostat (Thermo Fisher Scientific, Waltham, MA, USA) at -20°C; 5- $\mu\text{m}$ -thick sections were collected on Superfrost® Plus Slides (Thermo Fisher Scientific, Waltham, MA) and stored at -20°C until use. The slides were counterstained and mounted with Vectashield Mounting Medium with DAPI (4,6-diamidino-2-phenylindole; Vector Laboratories). Images were acquired with a Zeiss Axio Z1 fluorescence microscope (Carl Zeiss, Germany).

### **Flow cytometry analysis**

Phenotypic characterization was performed using the LSRFortessa instrument (Becton Dickinson) for murine cells. For analysis, FlowJo software (Tree Star Inc.) was used. TC1/Luc and spontaneous MMTV-PyMT oral tumors were digested in RPMI medium (Gibco, Invitrogen, Cergy Pontoise, France) supplemented with 1 mg/mL collagenase IV (Sigma) for 30 minutes at 37°C, entirely resuspended in PBS supplemented with 0.5% BSA/2 mmol/L EDTA (FACS buffer) and filtered using a 70- $\mu\text{m}$  cell strainer (BD Biosciences). Blood was drawn, and the cells were lysed in RBC lysis buffer containing 0.15 mol/L NH<sub>4</sub>Cl, 0.01 mmol/L KHCO<sub>3</sub>, and 0.1 mmol/L EDTA. Surface staining was performed by incubating 50  $\mu\text{L}$  of the cell suspension (one tenth of the total) with 1  $\mu\text{g}/\text{mL}$  purified anti-CD16/32 (2.4G2; BD Biosciences) for 10 minutes at 4°C followed by incubation with an appropriate dilution of specific surface antibodies for an additional 20 minutes. Dead cells were excluded using LIVE/DEAD Fixable Stain (Life Technologies) according to the manufacturer's instructions. Forward and side scatter parameters were used for doublet exclusion. After incubation, the cell suspensions were washed once in FACS buffer. The CCL2-binding assay was performed as previously described (17). Briefly, after surface staining, the cells were incubated in the dark for 45 minutes at 37°C in RPMI medium supplemented with GlutaMAX containing 25 nmol/L murine CCL2<sup>AF647</sup>(Almac

Sciences) and then washed with FACS buffer. For INF $\gamma$  and TNF $\alpha$  staining, cells were preincubated for 2 h with a cell activation cocktail containing Brefeldin A according to the manufacturer's instructions (BioLegend). After surface staining, the cells were fixed in 4% paraformaldehyde for 20 minutes, washed twice in Perm/Wash solution (BD Biosciences), incubated for 10 minutes with 1  $\mu$ g/mL purified anti-CD16/32 in Perm/Wash at room temperature, and incubated for 30 minutes in Perm/Wash in the presence of anti-INF $\gamma$  or anti-TNF $\alpha$ . For intracellular staining, the Foxp3/Transcription Factor Staining Buffer Set, anti-Foxp3 and anti-CTLA4 were used according to the manufacturers' instructions. Samples were washed in FACS buffer before acquisition. Calculation of the absolute numbers of different cell populations was performed by adding a fixed number (10,000) of nonfluorescent 10- $\mu$ m Polybead Carboxylate Microspheres (Polysciences) to each vial according to the following formula: number of cells = number of acquired cells  $\times$  10,000/number of acquired beads. The number of cells obtained for each sample was extrapolated to the whole organ. The panel of antibodies used comprised the following: anti-CD11b (clone M1/70), anti-Ly6C (clone AL-21), anti-Ly6G (clone 1A8), anti-NK1.1 (clone PK136), anti-I-Ab (clone AF6-120.1), anti-CD11c (clone HL3), anti-Siglec-F (clone E50-2440), anti-CD103 (clone M290), anti-CD45 (clone 30-F11), anti-CD4 (clone RM4-5), anti-CD3 (clone 145-2C11), anti-CD8 (clone 53-6.7), anti-CD25 (clone PC61), anti-CD64 (clone X54-5/7.1), anti-TNF $\alpha$  (clone MP6-XT22), anti-INF $\gamma$  (clone XMG1.2), anti-CTLA4 (clone UC10-4F10-11), anti-TGF $\beta$  (clone TW7-16B4), anti-Foxp3 (clone MF23; Pharmingen, BD Bioscience), anti-CD206 (clone C068C2; Biolegend) and anti-CCR2 (clone 475301; R&D systems, Minneapolis, MN, USA).

### **CCL2 ELISA**

The levels of CCL2 in cell supernatants and mouse sera were evaluated by ELISA using Mouse Quantikine ELISA Kits from R&D Systems.

### **Quantitative RT-PCR**

RNA was extracted from cells and tumor samples using the Qiagen RNeasy kit. The samples were treated with DNase-I (Qiagen), and RNA was retrotranscribed using the Bio-Rad I-Script kit. qRT-PCR analysis of CCL2 was performed using SYBR Green Mix (Applied Biosystems, Foster City, CA, USA) and the GeneAmp 7900HT Sequence Detection System (Applied Biosystems) as previously described (23).

### **Generation of the CCL2-deleted TC1/Luc cell line**

The genomic TC1/Luc cell line was edited using CRISPR-CAS9 technology to disrupt the *Ccl2* gene. The *Ccl2* mouse gene knockout via CRISPR kit (product number KN302782, Origene, Rockville, MD, USA) was used to knockout a region of the *Ccl2* gene and knockin a functional cassette containing GFP and the puromycin-resistance gene. Briefly, TC1/Luc cells were co-transfected with donor template DNA and pCas-guide plasmids using Lipofectamine 2000 (Thermo Fisher Scientific, USA), sorted for GFP expression, cultured for 7 weeks and then selected for puromycin resistance. Individual cell colonies were isolated by limiting dilution. Supernatants of clones were screened for CCL2 levels by ELISA, and CCL2-negative clones were

selected.

### **Tumor-macrophage co-cultures**

The TC1/Luc and RAW264.7 cells were mock-treated or irradiated at 7.5Gy and then respectively seeded into the lower and upper chambers of 6.5 mm transwells with a 0.4 µm Pore Polycarbonate Membrane Insert (Corning, NY, USA). The number of cells plated was adjusted considering the proliferation rate and the response to RT to yield an approximately equivalent number of cells regardless of the radiation dose delivered and the growth time. After 48 h of incubation, cell media were collected and analyzed by ELISA, and the mRNAs were separately extracted from TC1/Luc and Raw264.7 cells and analyzed by RT-qPCR.

### **Cytokine/chemokine array**

The cytokine and chemokine levels in tumor tissues were profiled using the Mouse Cytokine Array/Chemokine Array 31-Plex (ref. MD-31) at Eve Technologies Corporation (Calgary, AB, Canada). Protein extracts from tumor tissues were prepared by homogenization in RIPA buffer (Sigma-Aldrich, USA) containing a protease inhibitor cocktail (Roche, Basel, Switzerland) using Biomasher disposable homogenizers (Nippi, Tokyo, Japan). Protein extracts were diluted at 4 µg/µl, and the multiplex immunoassay Mouse Cytokine Array/Chemokine Array 32-Plex (Milliplex, Merck Millipore, USA) was analyzed with the BioPlex 200 instrument (Bio-Rad, USA).

### **Statistical analyses**

Statistical analyses were performed using Prism Version 7 (GraphPad, La Jolla, CA, USA). Survival data were analyzed using the Kaplan-Meier and log-rank tests for survival distribution. The bioluminescent signal (serving as a measurement of tumor size), immune infiltrate and tumor perfusion levels were analyzed using appropriate tests. Accordingly, multigroup analyses of variances were performed using one-way or two-way ANOVA followed by Sidak's or Tukey's multiple comparisons tests, respectively, or the Kruskal-Wallis test followed by Dunn's multiple comparisons test. For simple comparison analysis, unpaired Student's t-test was used to compare parametric distributions, and the Mann-Whitney test was used to compare nonparametric distributions. \*: p<0.05; \*\*: p<0.01; \*\*\*: p<0.001; \*\*\*\*: p<0.0001; ns=not significant.

## **RESULTS**

### **Radiotherapy induces the CCR2-dependent recruitment of monocytes into the tumor.**

Orthotopic inoculation of the TC1/Luc cell line was performed at a submucosal site of the inner lip in syngeneic wild-type (WT, *Ccr2*<sup>+/+</sup>) and *Ccr2*<sup>-/-</sup> mice to mimic an HPV-related oral cancer as described previously (18). Using the same model and irradiation treatment (**Fig 1A**), we showed here that the lack of stromal CCR2 improved the survival rate after localized RT (**Fig 1B**; median survival gain after RT for WT= 3 days, for *Ccr2*<sup>-/-</sup>= 6.5 days), which was associated with a reduction in tumor burden (**Fig S1A**). RT induced a transient CCR2-dependent increase

of classical Ly6C<sup>high</sup> monocytes (Ly6C<sup>high</sup> Mo) in the blood that was not observed after the local irradiation of tumor-free mice, indicating that the increase in blood Ly6C<sup>high</sup> Mo was dependent on irradiation of the tumor (**Fig 1C**). We next monitored the impact of RT on Ly6C<sup>high</sup> Mo and macrophage subsets within the tumor according to the gating strategy depicted in **Fig S1B**. The Ly6C<sup>high</sup> monocytosis induced by RT was associated with a massive and transient accumulation of Ly6C<sup>high</sup> Mo into the tumor, a higher CD64 expression and a subsequent accumulation of Ly6C<sup>low/-</sup> CD64<sup>+</sup> macrophages, suggesting that the latter mainly arose from the differentiation of Ly6C<sup>high</sup> Mo between days 3 and 5 post-RT (**Fig 1D**). CCR2 deficiency resulted in a severe impairment of both monocyte and macrophage accumulation on day 5 post-RT (**Fig 1E**). Newly infiltrated macrophages in WT mice displayed a higher proportion of I-Ab<sup>+</sup> cells, while CD206 was expressed at lower levels in these mice than in nonirradiated mice (**Fig 1F**). This activation profile was severely impaired in *Ccr2*<sup>-/-</sup> mice, with a lower expression of I-Ab and CD206 on the few infiltrated macrophages detected in these mice (**Fig 1F**). Histological analysis of MacBlue transgenic mice inoculated with tdTomato TC1 cells unveiled that the accumulation of ECFP<sup>+</sup> monocytes/macrophages mainly occurred at the tumor periphery after RT and was not observed in MacBlue x *Ccr2*<sup>-/-</sup> mice (**Fig S1C**). Overall, our results suggest that local tumor irradiation induces a CCR2-dependent increase of monocytes in the blood that subsequently infiltrate the tumor and progressively differentiate into macrophages.

#### **Radiotherapy induces the recruitment of CCR2<sup>+</sup> Tregs.**

We recently demonstrated that CCR2 represents an important homing receptor of Tregs toward the tumor and that a large fraction of Tregs are CCR2<sup>+</sup> in human HNSCC (17). In this orthotopic model of HNSCC, RT, together with an increased CCR2-dependent tumor infiltration of monocytes/macrophages, mediated a significant increase in CD4<sup>+</sup> conventional T cells (Tconvs) and Tregs in RT vs untreated tumors at 5 days post-treatment (**Fig 2A**). In the TC1/Luc model, the accumulation of Tconvs and Tregs was severely reduced in *Ccr2*<sup>-/-</sup> mice, in accordance with our previous study (**Fig 2A**) (17). In agreement with the CCR2-mediated recruitment of Tregs to irradiated tumors, the proportion of the CCR2<sup>+</sup> Treg subset was increased in WT mice following RT, while the percentage of CCR2<sup>+</sup> Tconvs was not significantly changed (**Fig 2B**). To investigate the effect of Tregs following RT in this HNSCC tumor model, we selectively depleted Tregs using Foxp3-DTR mice. Diphtheria toxin (DTx) treatment was started on day 2 after irradiation to fully impair RT-induced Treg recruitment (**Fig 2C**). Treg depletion in irradiated tumor-bearing mice reduced the tumor burden compared to that in non-depleted control mice (**Fig 2D**), confirming that Tregs limit RT efficacy. RT-induced accumulation of macrophages and Tregs was also confirmed in a spontaneous model of HNSCC, using male PyMT-ChOva mice that develop salivary tumors, suggesting that this observation is not restricted to engrafted models (**Fig 3**) (22).

#### **Radiotherapy triggers myeloid-associated cytokine secretion.**

To better understand the mechanisms underlying RT-mediated cell recruitment, we

investigated the effect of RT on CCL2 production. Local irradiation of tumor-bearing mice induced a transient increase in the serum CCL2 concentration at 3 days post-treatment (**Fig 4A**), which directly correlated with the Ly6C<sup>high</sup> Mo release into the blood (**Fig 1C**). In the absence of a tumor, the serum CCL2 concentration was not increased after RT (**Fig 4B**), while CCL2 accumulation was still detectable after irradiation of TC1/Luc tumor-bearing *Ccl2*<sup>-/-</sup> mice, indicating that the circulating CCL2 mainly originated from the tumor cells (**Fig S2A**). In contrast, no serum CCL2 accumulation was observed in either WT or *Ccl2*<sup>-/-</sup> mice bearing CCL2 knockdown (*Ccl2*<sup>-/-</sup>) TC1/Luc cells (**Fig S2B**). These results suggest that TC1/Luc tumor cells represent the main source of CCL2 production after RT rather than stromal cells. In the tumor, increased CCL2 transcription was detected by quantitative PCR 3 days after RT and was maintained on day 5 (**Fig S2C**). *In vitro*, when TC1/Luc tumor cells were co-cultured with the macrophage cell line RAW264.7, CCL2 secretion was increased and peaked when both TC1/Luc and RAW264.7 cells were exposed to ionizing radiation (**Fig 4C**), indicating that secreted factors from irradiated monocytes/macrophages further contribute to CCL2 upregulation at both the mRNA (**Fig S2D**) and secreted protein levels (**Fig 4C**). We next performed cytokine profiling on whole-tumor extracts and compared the levels of a set of cytokine and growth factors relevant to monocyte-derived cell recruitment and differentiation in nonirradiated control tumors and irradiated tumors at 5 days post-RT, when macrophages and Tregs were accumulated into irradiated tumors (**Fig 4D**). Among the cytokines and growth factors analyzed, CCL2 accumulation was confirmed at 5 days after RT. In addition, the IL3, GM-CSF, TNF $\alpha$  and IFN $\gamma$  levels significantly increased after RT, while the levels of M-CSF were similar to those in nonirradiated tumors. We concluded that local RT induces the secretion of CCL2 by tumor cells favoring the recruitment of Ly6C<sup>high</sup> Mo into the tumor, associated with an increased production of myeloid-cell related cytokines and growth factors involved in survival and differentiation.

### **TNF $\alpha$ limits the efficacy of RT in a Treg-dependent manner.**

We speculated that the co-recruitment of Tregs and monocytes following RT might favor the crosstalk between these two subsets. TNF $\alpha$  is known to have a direct effect on Treg function (24, 25) and was found to be upregulated in irradiated tumors (**Fig 4D**). In the tumor, Ly6C<sup>high</sup> Mo and TAMs represented important TNF $\alpha$  producers. The production of this cytokine was maintained in the newly infiltrated cells that accumulated 5 days after RT (**Fig 5A**). Anti-TNF $\alpha$  treatment after irradiation strongly improved the efficacy of RT (**Fig 5B**), while the effect of anti-TNF $\alpha$  was abrogated in Foxp3-DTR mice (**Fig 5C**), suggesting that the antitumor effect of anti-TNF $\alpha$  was mediated by Tregs. Anti-TNF $\alpha$  treatment reduced the Tregs frequency among CD4<sup>+</sup> T cells following RT (**Fig 5D**) and significantly reduced TGF $\beta$  expression by Tregs (**Fig 5E**), while CTLA4 expression was not modified (**Fig S3A**). Conventional CD4<sup>+</sup> and CD8<sup>+</sup> T cell infiltration was not modulated by anti-TNF $\alpha$  (**Fig S3B**), but RT increased the proportion of IFN $\gamma$ -producing CD8<sup>+</sup> T cells only when mice were treated with anti-TNF $\alpha$  (**Fig 5F**). Our results suggest that RT induces the CCR2-dependent accumulation of TNF $\alpha$ -producing myeloid cells

that activate Tregs and dampen the CD8<sup>+</sup> T cell response to ionizing radiation via TGF $\beta$  production.

### **Tregs interact with monocytes/macrophages in irradiated tumors.**

To further investigate the mechanism of Treg/monocyte crosstalk, we performed live imaging using intravital biphoton microscopy. Using MacBlue x Foxp3-EGFP double transgenic mice, we monitored the dynamic interactions of co-recruited monocytes/macrophages and Tregs within irradiated tumors 5 days after RT, at the time Tregs accumulated within the tumor. Clusters of monocytes/macrophages were present in close proximity to Treg cells (**Fig 6A**), and Tregs displayed multiple interactions with monocytes/macrophages (**Fig 6A** and **Supplemental Video 1**). Treatment with an anti-CD25 antibody is known to neutralize Treg activity without depleting the cell population (**Fig S4A**) (26). Anti-CD25 neutralized-Tregs displayed an increased mean velocity compared to that of IgG-treated controls (**Fig 6B**). While the rate of Treg interactions with monocytes/macrophages was not affected (**Fig 6C**), the duration of these interactions was significantly reduced in anti-CD25-treated mice likely explaining to the higher speediness of Tregs (**Fig 6D**). The very low number of Tregs in nonirradiated mice prevented us from analyzing their potential interactions with monocytes/macrophages. Anti-CD25 treatment was not sufficient to improve the RT effect (**Fig S4B-C**), but the altered pattern of interaction between Tregs and monocytes/macrophages upon CD25 inhibition was associated with an altered activation profile, as depicted by the reduced expression of major histocompatibility complex (MHC) class II molecules (I-Ab) in both tumor Ly6C<sup>high</sup> Mo and TAMs (**Fig 6E-F**), suggesting that Treg-monocyte/macrophage crosstalk occurs via direct cell-to-cell interactions.

## **DISCUSSION**

It is well recognized that RT severely impacts the TME and tumor immune response (27). Radiation promotes the recruitment of inflammatory cells into the TME but can also attract immunosuppressive cells (28). Our data, obtained using an orthotopic model of HPV-associated oral cancer, indicates that a marked influx of Ly6C<sup>high</sup> Mo, driven by the CCL2/CCR2 axis, is observable 3 days after a single exposure to 7.5Gy of ionizing radiation. Our observation on Ly6C<sup>high</sup> Mo mobilization is in accordance with others made using subcutaneous models of pancreatic (13) colon and lung adenocarcinoma (14) and with intramuscular models of colon adenocarcinoma, glioblastoma and lung carcinoma (12) with different RT regimens (15-20Gy), suggesting that the CCL2/CCR2-mediated recruitment of Ly6C<sup>high</sup> Mo can be a general mechanism that follows tumor exposure to ionizing radiation, at least at high doses (>7.5Gy). This sub-optimal RT regimen was chosen in order to monitor the added-value of the combined immunotherapy targeting CCR2 axis. Unpublished data (data not shown in Connolly *et al.* (12)) indicate that anti-CCR2/CCR5 treatment is ineffective at doses of 5x5Gy but synergizes with RT at 1x15Gy, indirectly suggesting that the mechanism of CCR2-mediated immunosuppressive cell recruitment could be different at lower and/or fractionated doses.

Nevertheless, it remains to be clearly elucidated whether CCR2-mediated recruitment occurs at lower RT doses, and especially after multiple RT exposures, to more closely recapitulate fractionated RT regimes in the clinical setting.

The mechanism was shown to involve the induction of increased CCL2 expression by irradiated tumor cells based on the following: 1 – CCL2 was still detectable and increased after RT when TC1/Luc cells were engrafted into *Ccl2*<sup>-/-</sup> mice; 2 – no upregulation of CCL2 was detectable in the blood of mice engrafted with a *Ccl2*<sup>-/-</sup> cell line (in line with Kalbasi *et al.* (13)) or in the blood of tumor-free mice after RT; and 3 – CCL2 was upregulated in tumor cells *in vitro* after RT. CCL2 upregulation in irradiated tumor cells is likely enhanced by the release of soluble factors from TAMs, as suggested by the tumor-macrophage co-culture experiments. Such mediators could include IL-6 (29) and type I interferons (14). Further experiments would be necessary to confirm whether primary tumor-monocytes as well as other stromal cells might enhance CCL2 upregulation after irradiation.

Our work clearly demonstrates that not only Ly6C<sup>high</sup> Mo but also Tregs recruitment to the tumor after RT involves the CCL2/CCR2 pathway. The intratumor Treg strongly accumulated 5 days post-RT while the Treg accumulation in irradiated *Ccr2*<sup>-/-</sup> mice was severely reduced. We cannot exclude that the increase in Tregs was partly due to the local proliferation of intratumor Tregs after radiation, as this observation was recently described using different tumor models (30). Nevertheless, the lack of increase in Tregs in irradiated tumors from *Ccr2*<sup>-/-</sup> mice and the increased proportion of CCR2-expressing Tregs in WT mice after RT are supportive of a significant role of CCR2-mediated Treg recruitment in the tumor bed.

The co-recruited monocytes/macrophages and Tregs displayed dynamic interactions within the irradiated tumor tissue, suggesting a direct cell-to-cell mediated crosstalk between these two subsets. Anti-CD25 treatment strongly reduced the contact duration between these subsets, showing that these interactions are not random but rather guided by a specific activation state of the different subsets. Recently, Romano *et al.* showed that expanded Tregs polarize *in vitro* monocytes toward alternatively activated macrophages (24). In the tumor context, we observed that functional Tregs induce monocyte/macrophage activation by upregulating the expression of MHC class II molecules, suggesting that they might favor direct T cell receptor (TCR) engagement. In this system, anti-CD25 treatment did not improve the RT efficacy showing that reducing the duration of the interaction between Tregs and monocytes/macrophages is not sufficient to abrogate their immunosuppressive activity. Whether local CCL2 production favors physical interactions between the two subsets deserves further investigation. Among local cytokines produced following RT, TNF $\alpha$  was previously demonstrated to exert a radioprotective effect, which was proposed to occur via VEGF production by TAMs (31). We further demonstrated that TNF $\alpha$  neutralization enhances tumor response to RT by reducing Treg frequency and TGF $\beta$  production. Considering the role of TGF $\beta$  in Treg-mediated immunosuppressive activity (32), the activation of this axis is strongly relevant to the radioprotective actions of Tregs. Among these protective actions, we observed that anti-TNF $\alpha$  increased the frequency of IFN $\gamma$ -producing CD8<sup>+</sup> T cells after RT. While CTLA4 expression was increased in Tregs following RT, its expression was not modified by anti-TNF $\alpha$ ,

suggesting that TNF $\alpha$  might regulate specific pathways of Treg activation. Several pieces of data have indicated that TNF $\alpha$  induces more specific signaling in Tregs via TNFR2 to maintain their suppressive activity (25, 33, 34). Deciphering the pathway of Treg activation following RT is crucial considering the potential of combined immunotherapies targeting Tregs with RT. Considering the cytotoxic effect of TNF $\alpha$  (35), one could assume that a shortened anti-TNF $\alpha$  treatment might efficiently block Treg accumulation while avoiding inhibition of CD8<sup>+</sup> T cell activity. In contrast to most cancers, paradoxical observations have been gathered on the role of Tregs in patients with HNSCC, suggesting that tumor Treg density correlate with increased survival (36). This discrepancy is poorly understood, and some observations suggest that Tregs suppress the induction of a chronic inflammatory state in the tissue (37). However, these hypotheses are still being debated, as other research showed no such correlation (38). Our data clearly indicate that Tregs play a detrimental role in the response to RT, as their depletion increases RT efficacy. Thus, targeting Tregs could be an interesting therapeutic approach to enhance the RT index, as previously suggested (see Liu *et al.* (39) for a review).

The results of our study offer interesting perspectives. Our data provide strong evidence for the thus far poorly studied crosstalk between adaptive and innate immune system components and indicate that impacting the monocyte/Treg interaction after RT could increase the antitumor effect of RT. The extent of CCL2 and TNF $\alpha$  production was heterogenous between tumors following RT, possibly reflecting the differential response to radiation. It would thus be interesting to evaluate the prognostic value of these cytokines. As modulators of CCL2 and CCR2 are already being tested in clinical settings, translating the results from this study into the clinic is conceivable. An alternative (and potentially synergistic) approach could be to use anti-TNF $\alpha$  or anti-TGF $\beta$  therapeutics to overcome the immunosuppressive effects of Tregs and thus potentiate the effects of RT. Our data underline the relevance of using combined strategies to improve the biological efficacy of ionizing radiation-based therapies and limit the toxicities related to dose escalation. Indeed, de-intensifying treatments to avoid late toxicity is a foremost goal and an active area of research. The use of RT in combination with CCL2/CCR2 and anti-TNF $\alpha$  modulators represents a promising approach to achieve such goals.

## **ACKNOWLEDGMENTS**

The authors wish to thank the "NAC" animal facility for their assistance with mouse breeding and the Plateforme d'Évaluation Préclinique (PFEP) for providing animal care.

## **CONTRIBUTIONS**

M.M., A.B. and E.D. initiated the project concept and supervised the project. A.B., M.M. and P.L.L. conceived and designed the experiments. M.M., P.L.L., P.H., M.G.D.T., M.L., K.B. and A.B. performed the experiments. C.Cl., B.S., C.Co. and E.D. provided suggestions and technical support. M.M., A.B. and P.H. wrote the manuscript. All authors discussed the results and commented on the manuscript.

## REFERENCES

1. Caudell JJ, Torres-Roca JF, Gillies RJ, Enderling H, Kim S, Rishi A, et al. The future of personalised radiotherapy for head and neck cancer. *Lancet Oncol* 2017;18:e266-e73.
2. Demaria S, Golden EB, Formenti SC. Role of Local Radiation Therapy in Cancer Immunotherapy. *JAMA Oncol* 2015;1:1325-32.
3. Vacchelli E, Bloy N, Aranda F, Buque A, Cremer I, Demaria S, et al. Trial Watch: Immunotherapy plus radiation therapy for oncological indications. *Oncoimmunology* 2016;5:e1214790.
4. Hettich M, Lahoti J, Prasad S, Niedermann G. Checkpoint Antibodies but not T Cell-Recruiting Diabodies Effectively Synergize with TIL-Inducing gamma-Irradiation. *Cancer Res* 2016;76:4673-83.
5. Derer A, Frey B, Fietkau R, Gaipl US. Immune-modulating properties of ionizing radiation: rationale for the treatment of cancer by combination radiotherapy and immune checkpoint inhibitors. *Cancer Immunol Immunother* 2016;65:779-86.
6. Frey B, Ruckert M, Weber J, Mayr X, Derer A, Lotter M, et al. Hypofractionated Irradiation Has Immune Stimulatory Potential and Induces a Timely Restricted Infiltration of Immune Cells in Colon Cancer Tumors. *Front Immunol* 2017;8:231.
7. Fontenot JD, Gavin MA, Rudensky AY. Foxp3 programs the development and function of CD4+CD25+ regulatory T cells. *Nat Immunol* 2003;4:330-6.
8. Ugel S, De Sanctis F, Mandruzzato S, Bronte V. Tumor-induced myeloid deviation: when myeloid-derived suppressor cells meet tumor-associated macrophages. *J Clin Invest* 2015;125:3365-76.
9. Waniczek D, Lorenc Z, Snietura M, Wesecki M, Kopec A, Muc-Wierzgon M. Tumor-Associated Macrophages and Regulatory T Cells Infiltration and the Clinical Outcome in Colorectal Cancer. *Arch Immunol Ther Exp (Warsz)* 2017;65:445-54.
10. Franciszkiewicz K, Boissonnas A, Boutet M, Combadiere C, Mami-Chouaib F. Role of chemokines and chemokine receptors in shaping the effector phase of the antitumor immune response. *Cancer Res* 2012;72:6325-32.
11. Conti I, Rollins BJ. CCL2 (monocyte chemoattractant protein-1) and cancer. *Semin Cancer Biol* 2004;14:149-54.
12. Connolly KA, Belt BA, Figueroa NM, Murthy A, Patel A, Kim M, et al. Increasing the efficacy of radiotherapy by modulating the CCR2/CCR5 chemokine axes. *Oncotarget* 2016;7:86522-35.
13. Kalbasi A, Komar C, Tooker GM, Liu M, Lee JW, Gladney WL, et al. Tumor-Derived CCL2 Mediates Resistance to Radiotherapy in Pancreatic Ductal Adenocarcinoma. *Clin Cancer Res* 2017;23:137-48.
14. Liang H, Deng L, Hou Y, Meng X, Huang X, Rao E, et al. Host STING-dependent MDSC mobilization drives extrinsic radiation resistance. *Nat Commun* 2017;8:1736.
15. Franklin RA, Liao W, Sarkar A, Kim MV, Bivona MR, Liu K, et al. The cellular and molecular origin of tumor-associated macrophages. *Science* 2014;344:921-5.
16. Qian BZ, Li J, Zhang H, Kitamura T, Zhang J, Campion LR, et al. CCL2 recruits inflammatory monocytes to facilitate breast-tumour metastasis. *Nature* 2011;475:222-5.
17. Loyher PL, Rochefort J, Baudesson de Chanville C, Hamon P, Lescaille G, Bertolus C, et al. CCR2 Influences T Regulatory Cell Migration to Tumors and Serves as a Biomarker of Cyclophosphamide Sensitivity. *Cancer Res* 2016;76:6483-94.

18. Mondini M, Nizard M, Tran T, Mauge L, Loi M, Clemenson C, et al. Synergy of Radiotherapy and a Cancer Vaccine for the Treatment of HPV-Associated Head and Neck Cancer. *Mol Cancer Ther* 2015;14:1336-45.
19. Wang Y, Kissenpennig A, Mingueneau M, Richelme S, Perrin P, Chevrier S, et al. Th2 lymphoproliferative disorder of LatY136F mutant mice unfolds independently of TCR-MHC engagement and is insensitive to the action of Foxp3+ regulatory T cells. *J Immunol* 2008;180:1565-75.
20. Ovchinnikov DA, van Zuylen WJ, DeBats CE, Alexander KA, Kellie S, Hume DA. Expression of Gal4-dependent transgenes in cells of the mononuclear phagocyte system labeled with enhanced cyan fluorescent protein using Csf1r-Gal4VP16/UAS-ECFP double-transgenic mice. *J Leukoc Biol* 2008;83:430-3.
21. Kim JM, Rasmussen JP, Rudensky AY. Regulatory T cells prevent catastrophic autoimmunity throughout the lifespan of mice. *Nat Immunol* 2007;8:191-7.
22. Engelhardt JJ, Boldajipour B, Beemiller P, Pandurangi P, Sorensen C, Werb Z, et al. Marginating dendritic cells of the tumor microenvironment cross-present tumor antigens and stably engage tumor-specific T cells. *Cancer Cell* 2012;21:402-17.
23. Henke PK, Pearce CG, Moaveni DM, Moore AJ, Lynch EM, Longo C, et al. Targeted deletion of CCR2 impairs deep vein thrombosis resolution in a mouse model. *J Immunol* 2006;177:3388-97.
24. Romano M, Fanelli G, Tan N, Nova-Lamperti E, McGregor R, Lechler RI, et al. Expanded Regulatory T Cells Induce Alternatively Activated Monocytes With a Reduced Capacity to Expand T Helper-17 Cells. *Front Immunol* 2018;9:1625.
25. Salomon BL, Leclerc M, Tosello J, Ronin E, Piaggio E, Cohen JL. Tumor Necrosis Factor alpha and Regulatory T Cells in Oncoimmunology. *Front Immunol* 2018;9:444.
26. Arce Vargas F, Furness AJS, Solomon I, Joshi K, Mekkaoui L, Lesko MH, et al. Fc-Optimized Anti-CD25 Depletes Tumor-Infiltrating Regulatory T Cells and Synergizes with PD-1 Blockade to Eradicate Established Tumors. *Immunity* 2017;46:577-86.
27. Frey B, Ruckert M, Deloch L, Ruhle PF, Derer A, Fietkau R, et al. Immunomodulation by ionizing radiation-impact for design of radio-immunotherapies and for treatment of inflammatory diseases. *Immunol Rev* 2017;280:231-48.
28. Weichselbaum RR, Liang H, Deng L, Fu YX. Radiotherapy and immunotherapy: a beneficial liaison? *Nat Rev Clin Oncol* 2017;14:365-79.
29. Wang X, Yang X, Tsai Y, Yang L, Chuang KH, Keng PC, et al. IL-6 Mediates Macrophage Infiltration after Irradiation via Up-regulation of CCL2/CCL5 in Non-small Cell Lung Cancer. *Radiat Res* 2017;187:50-9.
30. Muroyama Y, Nirschl TR, Kochel CM, Lopez-Bujanda Z, Theodoros D, Mao W, et al. Stereotactic Radiotherapy Increases Functionally Suppressive Regulatory T Cells in the Tumor Microenvironment. *Cancer Immunol Res* 2017;5:992-1004.
31. Meng Y, Beckett MA, Liang H, Mauceri HJ, van Rooijen N, Cohen KS, et al. Blockade of tumor necrosis factor alpha signaling in tumor-associated macrophages as a radiosensitizing strategy. *Cancer Res* 2010;70:1534-43.
32. Tran DQ. TGF-beta: the sword, the wand, and the shield of FOXP3(+) regulatory T cells. *J Mol Cell Biol* 2012;4:29-37.
33. Yang S, Wang J, Brand DD, Zheng SG. Role of TNF-TNF Receptor 2 Signal in Regulatory T Cells and Its Therapeutic Implications. *Front Immunol* 2018;9:784.

34. Zaragoza B, Chen X, Oppenheim JJ, Baeyens A, Gregoire S, Chader D, et al. Suppressive activity of human regulatory T cells is maintained in the presence of TNF. *Nat Med* 2016;22:16-7.
35. Larrick JW, Wright SC. Cytotoxic mechanism of tumor necrosis factor-alpha. *FASEB J* 1990;4:3215-23.
36. Lim KP, Chun NA, Ismail SM, Abraham MT, Yusoff MN, Zain RB, et al. CD4+CD25hiCD127low regulatory T cells are increased in oral squamous cell carcinoma patients. *PLoS One* 2014;9:e103975.
37. Al-Qahtani D, Anil S, Rajendran R. Tumour infiltrating CD25+ FoxP3+ regulatory T cells (Tregs) relate to tumour grade and stromal inflammation in oral squamous cell carcinoma. *J Oral Pathol Med* 2011;40:636-42.
38. Song JJ, Zhao SJ, Fang J, Ma D, Liu XQ, Chen XB, et al. Foxp3 overexpression in tumor cells predicts poor survival in oral squamous cell carcinoma. *BMC Cancer* 2016;16:530.
39. Liu S, Sun X, Luo J, Zhu H, Yang X, Guo Q, et al. Effects of radiation on T regulatory cells in normal states and cancer: mechanisms and clinical implications. *Am J Cancer Res* 2015;5:3276-85.

## FIGURE LEGENDS

**Figure 1: Radiotherapy induces the CCR2-dependent recruitment of monocytes into the tumor.**

**(A)** C57Bl/6 wild-type (WT, *Ccr2*<sup>+/+</sup>) and *Ccr2* KO (*Ccr2*<sup>-/-</sup>) mice were injected with TC1/Luc cells in their inner lip and then locally irradiated at 7.5Gy. Blood and tumor samples were collected at different time points as depicted in the schematic diagram. **(B)** Kaplan-Meier survival curves for mock- or radiotherapy (RT)-treated mice. The log-rank test was performed (n=8-15 mice/group from 3 independent experiments). **(C)** Numbers of Ly6C<sup>high</sup> monocytes in the bloodstreams of tumor-bearing WT (*Ccr2*<sup>+/+</sup>) and *Ccr2* KO (*Ccr2*<sup>-/-</sup>) mice and nontumor-challenged WT mice (Tumor-free) with or without RT treatment (n= more than 4 mice/group per time point from at least two independent experiments). **(D)** Left, representative Ly6C/CD64 dot plots of tumor-infiltrating monocytes/macrophages in nonirradiated (Ctrl) and irradiated (RT) mice at 3 and 6 days post-RT (the mean±SD percentages of cells in each gate are indicated, n=8 mice/group from two independent experiments). Right panels, numbers of tumor Ly6C<sup>high</sup> monocytes (Ly6C<sup>high</sup> Mo) and tumor-associated macrophages (TAMs) per mg. Two-way ANOVA with Tukey's multiple comparisons test was performed for RT vs nonirradiated mice at each time point (n=8-15 mice/group per time point from at least two independent experiments). **(E)** Absolute numbers of Ly6C<sup>high</sup> Mo and TAMs in WT and *Ccr2*<sup>-/-</sup> mice per mg at 5 days post-RT. One-way ANOVA with Sidak's multiple comparisons test was performed for RT vs nonirradiated mice at each time point (n=9-10 mice/group from three independent experiments). **(F)** Representative Ly6C/I-Ab (left panels) and Ly6C/CD206 (right panels) dot plots of tumor-infiltrating monocytes/macrophages in nonirradiated (Ctrl) and irradiated (RT) mice at 5 days post-RT (the mean±SD percentages of cells in each gate are indicated, n=6-8 mice/group from two independent experiments). For all panels: \*: p<0.05;

\*\* : p<0.01; \*\*\* : p<0.001; \*\*\*\* : p<0.0001.

**Figure 2: Radiotherapy induces the recruitment of CCR2<sup>+</sup> Tregs.**

**(A)** Left panels, representative dot plots of regulatory T cells (Tregs) in nonirradiated (Ctrl) and irradiated (RT) wild-type (WT, *Ccr2*<sup>+/+</sup>) mice at 5 days post-RT. Right panels, numbers of tumor Tregs and conventional CD4<sup>+</sup> T cells (Tconvs) per mg in WT and *Ccr2*<sup>-/-</sup> mice. One-way ANOVA with Sidak's multiple comparisons test was performed for RT vs nonirradiated WT and *Ccr2*<sup>-/-</sup> mice (n=9-14 mice/group from three independent experiments). **(B)** Histograms showing the expression of CCR2 on the surface of Tregs (left panel) in WT and *Ccr2*<sup>-/-</sup> mice and quantification of the percentages of CCR2<sup>+</sup> Tregs and Tconvs in nonirradiated and irradiated (RT) WT mice (right panel). One-way ANOVA with Sidak's multiple comparisons test was performed for Tconvs and Tregs in RT vs nonirradiated mice (n=13-16 mice/group from three independent experiments). **(C)** Representative dot plots (left panels) and quantification of the percentages (right panel) of Tregs in irradiated tumors from WT and Foxp3-DTR mice treated with diphtheria toxin (DTx). Unpaired Student's t-test was performed (n=9-18 mice/group from at least two independent experiments). **(D)** Tumor growth in WT and Foxp3-DTR mice treated with DTx (black arrows) was monitored by bioluminescence *in vivo* imaging. Data for WT Ctrl mice (WT+DTx) at day 7 are not indicated since mice were euthanized before this time point. One-way ANOVA with Sidak's multiple comparisons test was performed (n=6-18 mice/group from at least two independent experiments). For all panels: \*: p<0.05; \*\*: p<0.01; \*\*\*: p<0.001; \*\*\*\*: p<0.0001.

**Figure 3: Macrophages and Tregs accumulates in irradiated spontaneous oral tumors.**

Spontaneous oral tumors from MMTV-PyMT mice bearing fluorescent reporters for tumor cells (mCherry, red) and monocytes/macrophages (ECFP, light blue, the MacBlue reporter allows the specific visualization of tumor-associated monocytes/macrophages) were irradiated and analyzed 5 days later by flow cytometry **(A)** or confocal microscopy **(B)**. Two-way ANOVA with Sidak's multiple comparisons test was performed (n=3-6 mice/group from two independent experiments).

**Figure 4: Radiotherapy triggers myeloid-associated cytokine secretion.**

The CCL2 levels in the sera of mice engrafted with TC1/Luc tumor cells **(A)** and nontumor-challenged wild-type mice (Tumor-free) **(B)** were evaluated by ELISA at different time points after 7.5Gy irradiation (RT). **(C)** TC1/Luc and Raw 264.7 cells were mock-treated (NI=non-irradiated) or irradiated at 7.5Gy (IR) and then co-cultured in transwell chambers for 48h; the cell supernatants were then collected for ELISA (- = no cells; data from two independent experiments performed in triplicate). **(D)** Cytokine profiling of whole-tumor protein extracts performed 5 days after the treatment of WT mice with 7.5Gy irradiation. One-way ANOVA with Sidak's multiple comparisons test **(A and B)** or two-way ANOVA with Tukey's multiple comparisons test **(C)** and the Mann-Whitney test **(D)** were performed. For **A, B and D**: n=4-20 mice/group per time point out of at least two independent experiments. For all panels: \*: p<0.05; \*\*: p<0.01; \*\*\*: p<0.001; \*\*\*\*: p<0.0001.

**Figure 5: TNF $\alpha$  limits the efficacy of RT in a Treg-dependent manner.**

**(A)** Representative histograms of flow cytometry analyses of intracellular staining to evaluate TNF $\alpha$  levels in tumor Ly6C<sup>high</sup> Mo and TAMs from nonirradiated (Ctrl) and irradiated (RT) WT mice at 5 days post-RT. The mean $\pm$ SD of the percentage of TNF $\alpha$ <sup>+</sup> cells is indicated (n=6-10 mice from two independent experiments). Irradiated WT **(B)**, Foxp3-DTR and DTx-treated **(C)** mice were injected with a control (isotype) or neutralizing anti-TNF $\alpha$  Ab (aTNF $\alpha$ , black arrows), and tumor growth was monitored by *in vivo* imaging. Two-way ANOVA with Tukey's multiple comparisons test was performed (n=9-10 mice/group per time point out of at least two independent experiments). **(D)** Absolute numbers per mg (left panel) and percentages (right panel) of CD4<sup>+</sup> Tregs in tumors from WT mice treated with RT and/or anti-TNF $\alpha$ . **(E)** TGF $\beta$  expression in Tregs from tumors of WT mice treated with RT and/or anti-TNF $\alpha$  as quantified by flow cytometry. The mean $\pm$ SD of the percentage of TGF $\beta$ <sup>+</sup> is indicated. **(F)** Percentage of CD8<sup>+</sup> T cells expressing IFN $\gamma$  as detected by flow cytometry in tumors from WT mice treated with RT and/or anti-TNF $\alpha$ . One-way ANOVA with Sidak's multiple comparisons test was performed for **D**, **E** and **F** (n=6-9 mice/group out of two independent experiments). For all panels: \*: p<0.05; \*\*: p<0.01; \*\*\*: p<0.001.

**Figure 6: Tregs interact with monocytes/macrophages in irradiated tumors.**

Intravital biphoton microscopy analysis of explanted TC1/Luc tumors from MacBlue/Foxp3-EGFP mice was performed at 5 days after radiotherapy. **(A)** Time-lapse TPLSM image sequence from a representative field showing multiple interactions (red arrows) between Tregs (green) and monocytes (light blue). Scatter plots representing the quantification of Treg motility **(B)** and the rate **(C)** and duration **(D)** of Treg-monocyte/macrophage interactions in irradiated tumors from mice treated with anti-CD25 or control IgG (isotype) (data are pooled from 3-4 mice in each group). The expression of MHCII (I-Ab) on the surface of Ly6C<sup>high</sup> monocytes **(E)** and macrophages **(F)** was quantified by flow cytometry (n=12-17 mice/group out of three independent experiments). The Mann-Whitney test was performed for **B**, **C**, **D**, **E** and **F**. For all panels: ns: nonsignificant; \*: p<0.05; \*\*: p<0.01; \*\*\*: p<0.001; \*\*\*\*: p<0.0001.

**Supplementary Figure S1:** (A) Tumor growth was monitored by bioluminescence imaging in C57Bl/6 wild-type (WT, *Ccr2*<sup>+/+</sup>) or *Ccr2* KO (*Ccr2*<sup>-/-</sup>) mice locally irradiated or not at 7.5Gy (n=8-15 mice per group, two-way ANOVA with Sidak's multiple comparisons test was performed, \*\*: p<0.01). (B) Flow cytometry dot plots show the gating strategy to discriminate tumor myeloid subsets. (C) Confocal analysis of tumor cryosections of tdTomato TC1 tumor-bearing *Ccr2*<sup>+/+</sup> x MacBlue and *Ccr2*<sup>-/-</sup> x MacBlue mice showing the distribution of monocytes/macrophages (ECFP, light blue) in the tumor core and at the periphery.

**Supplementary Figure S2:** (A) The CCL2 levels in the sera of *Ccl2* KO (*Ccl2*<sup>-/-</sup>) mice engrafted with TC1/Luc tumor cells were evaluated by ELISA 3 days after 7.5Gy irradiation. The Mann-Whitney test was performed (n=3-10 mice/group from two independent experiments). (B) *Ccl2*<sup>-/-</sup> TC1/Luc cells generated by CRISPR-Cas9 were engrafted into *Ccl2*<sup>+/+</sup> or *Ccl2*<sup>-/-</sup> mice. The CCL2 serum levels were analyzed by ELISA 3 days after RT. Two-way ANOVA with Sidak's multiple comparisons test was performed (n=3-10 mice/group from two independent experiments). (C) qPCR analysis of CCL2 mRNA in tumors from WT mice at different time points after radiotherapy. Two-way ANOVA with Sidak's multiple comparisons test was performed (n=3-4 mice/group). (D) TC1/Luc and Raw 264.7 cells were mock-treated (NI=nonirradiated) or irradiated at 7.5Gy (IR) and then co-cultured in transwell chambers for 48h; RNA was then extracted for qPCR analysis (- = no cells). The Kruskal-Wallis test with Dunn's multiple comparisons test was performed (data are from three replicates and three independent experiments). For all panels: \*: p<0.05; \*\*: p<0.01.

**Supplementary Figure S3:** (A) The expression of CTLA4 on the surface of Tregs in tumors from WT mice treated with RT and/or anti-TNF $\alpha$  was quantified by flow cytometry. (B) Absolute numbers of Tconv CD4<sup>+</sup> (left panel) and CD8<sup>+</sup> cells (right panel) per mg in tumors from WT mice treated with RT and/or anti-TNF $\alpha$ . One-way ANOVA with Sidak's multiple comparisons test was performed for all panels (n=6-10 mice/group from two independent experiments). For all panels: \*: p<0.05; \*\*: p<0.01; \*\*\*: p<0.001.

**Supplementary Figure S4:** (A) Quantification of the percentages of Tregs and their mean fluorescence intensities (MFIs) of CD25 expression in the tumors of irradiated wild-type mice treated with anti-CD25 or a control isotype. Unpaired Student's t-test was performed (n=11-18 mice/group from three independent experiments). \*: p<0.05. (B) Tumor growth was monitored by bioluminescence imaging in C57Bl/6 wild-type mice locally irradiated or not at 7.5Gy (n=3-6 mice per group) and treated with anti-CD25 or control IgG (Ctrl). Two-way ANOVA with Sidak's multiple comparisons test was performed. (C) Kaplan-Meier survival curves for mock- or radiotherapy (RT)-treated mice. The log-rank test was performed (n=3-6 mice/group)

**Supplementary movie 1:** Intravital biphoton microscopy analysis of explanted TC1/Luc tumors from MacBlue/Foxp3-EGFP mice was performed at 5 days after radiotherapy. Time-lapse TPLSM video sequence from a representative field showing multiple interactions between Tregs and monocytes.

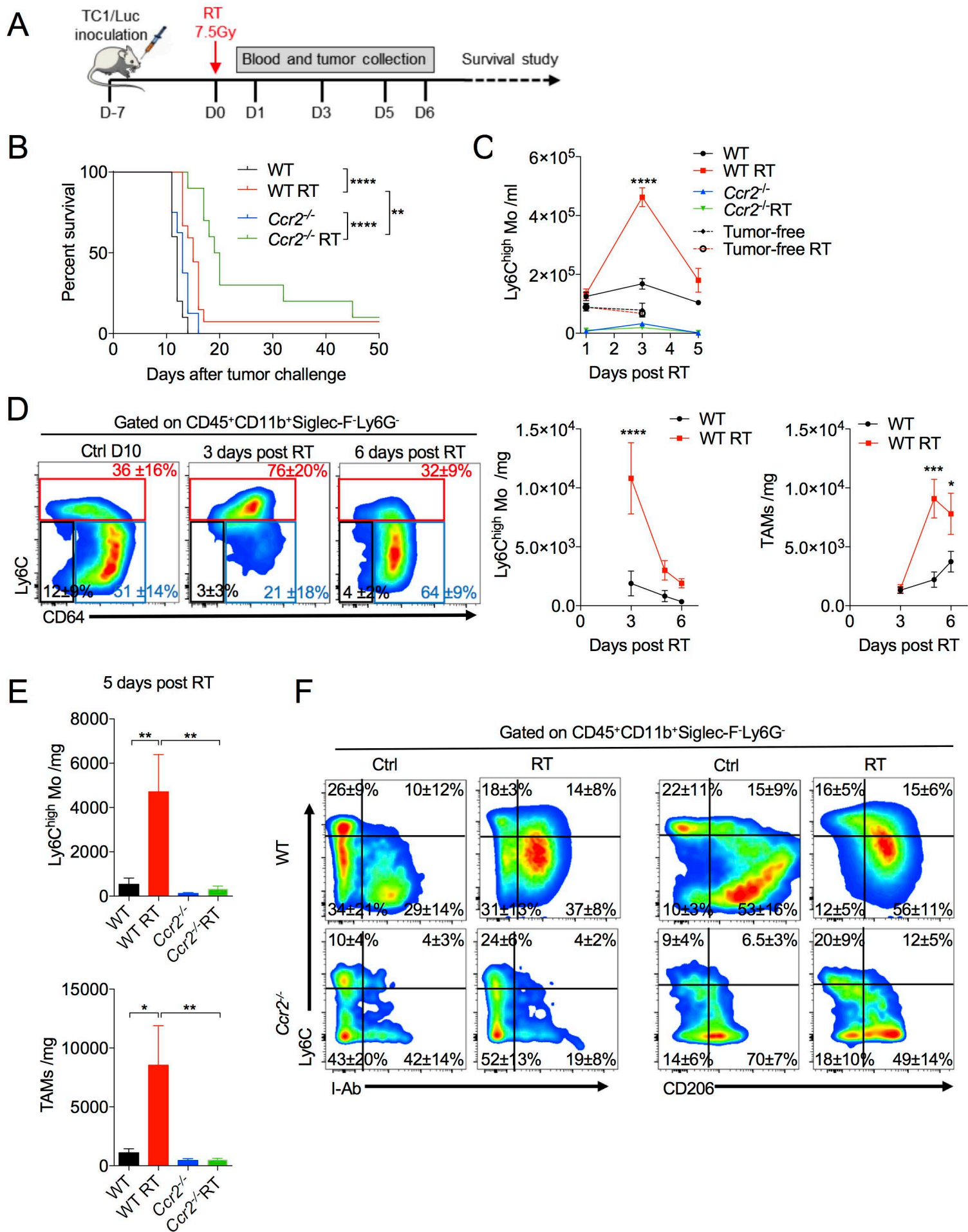


Figure 1



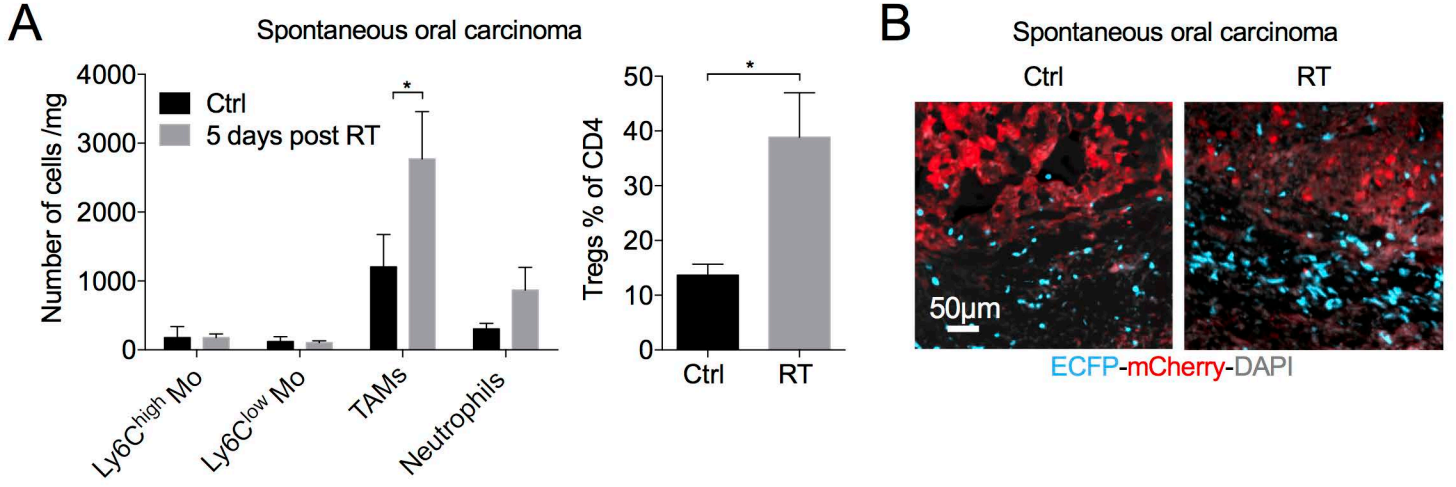


Figure 3

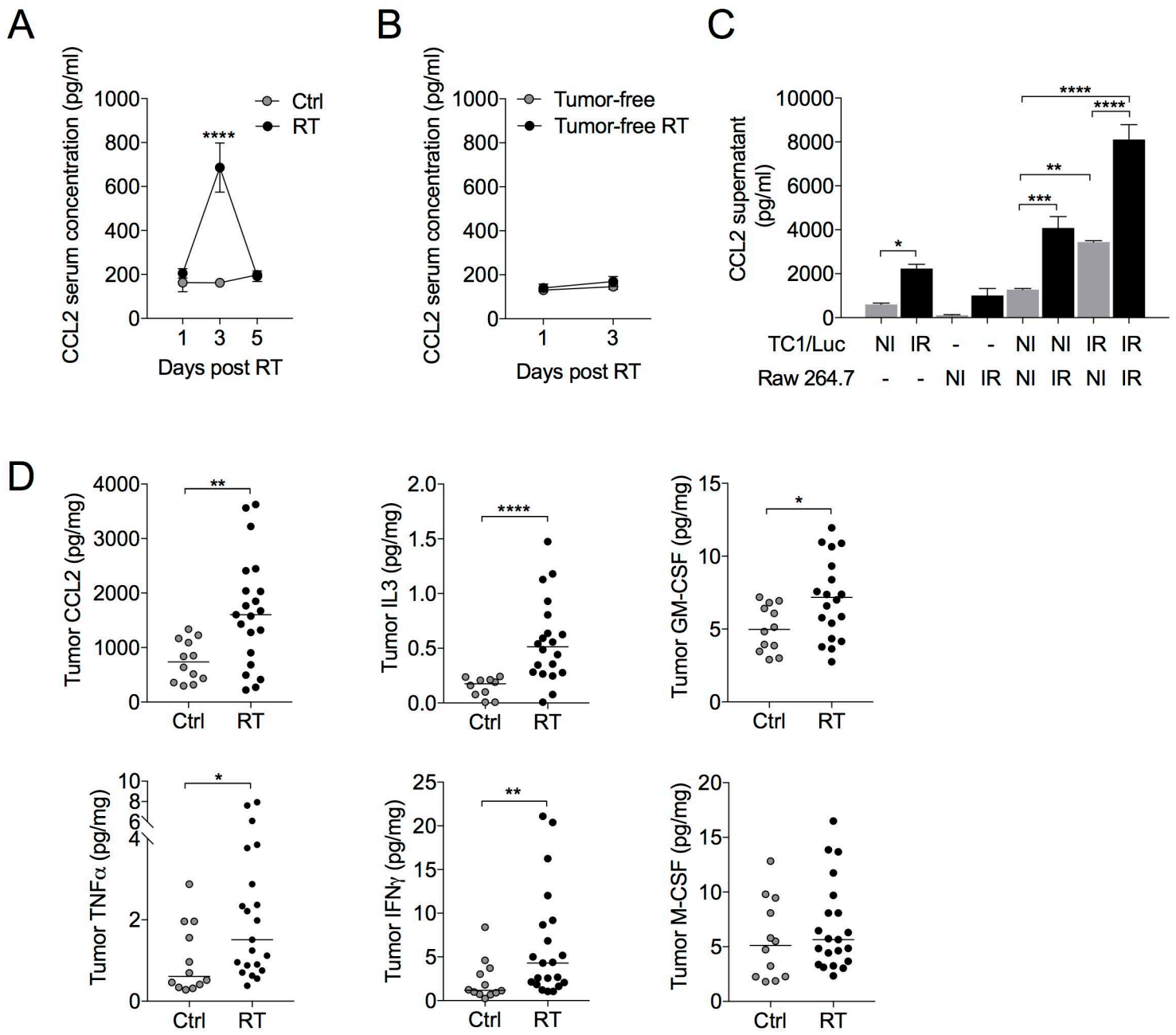


Figure 4

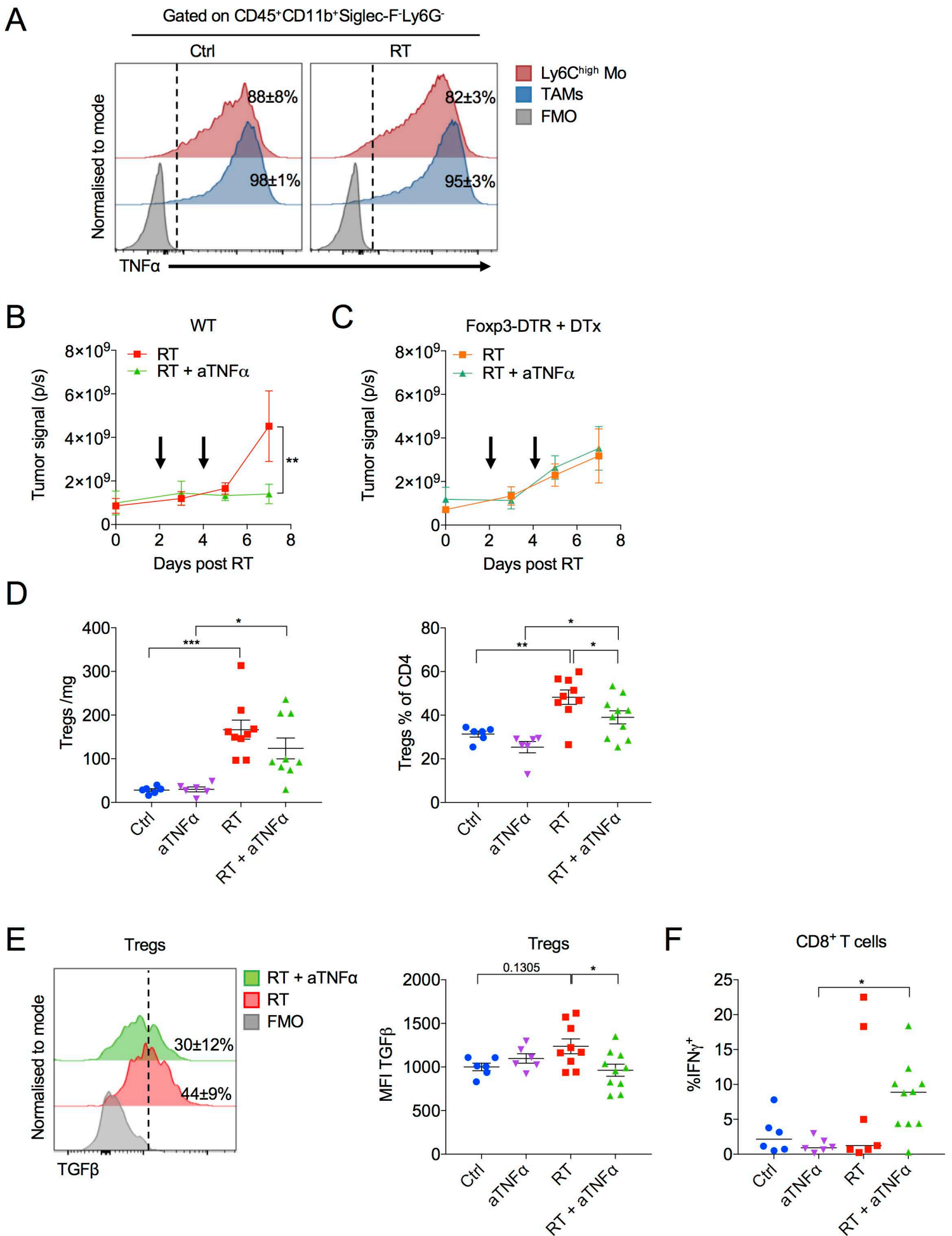


Figure 5

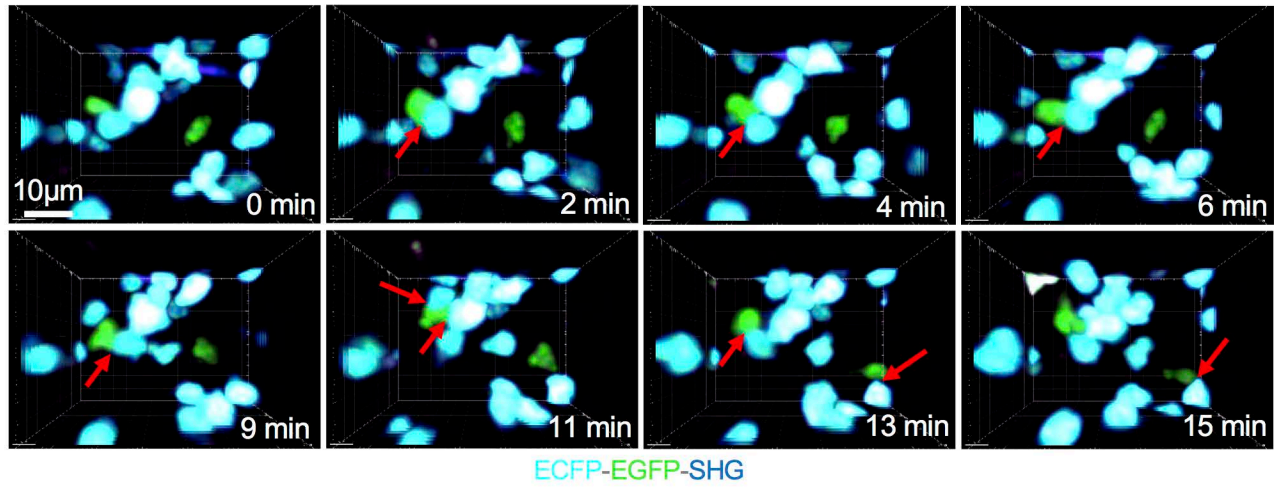
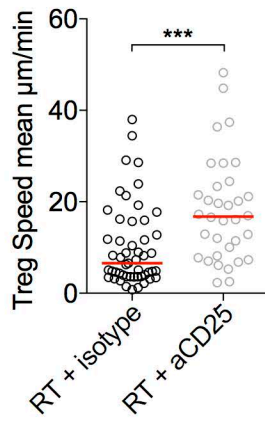
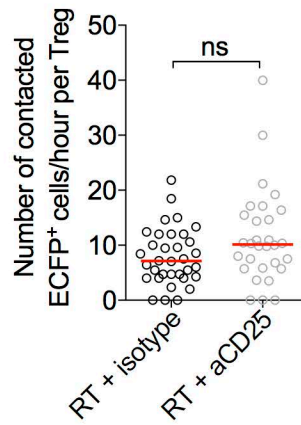
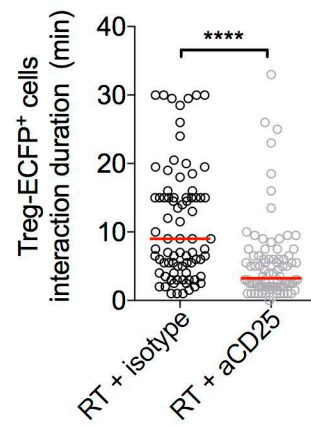
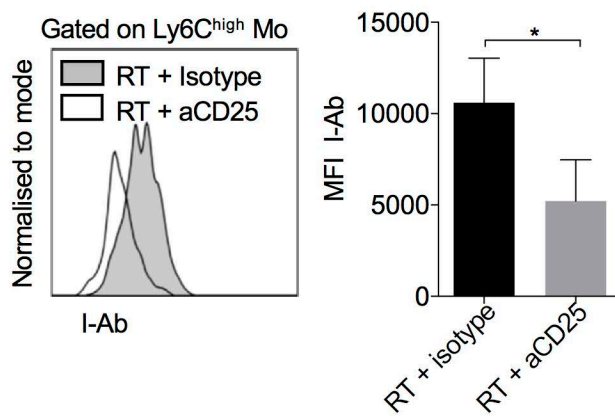
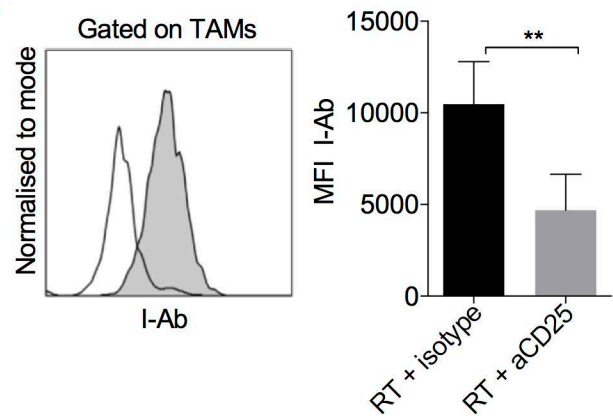
**A****B****C****D****E****F**

Figure 6

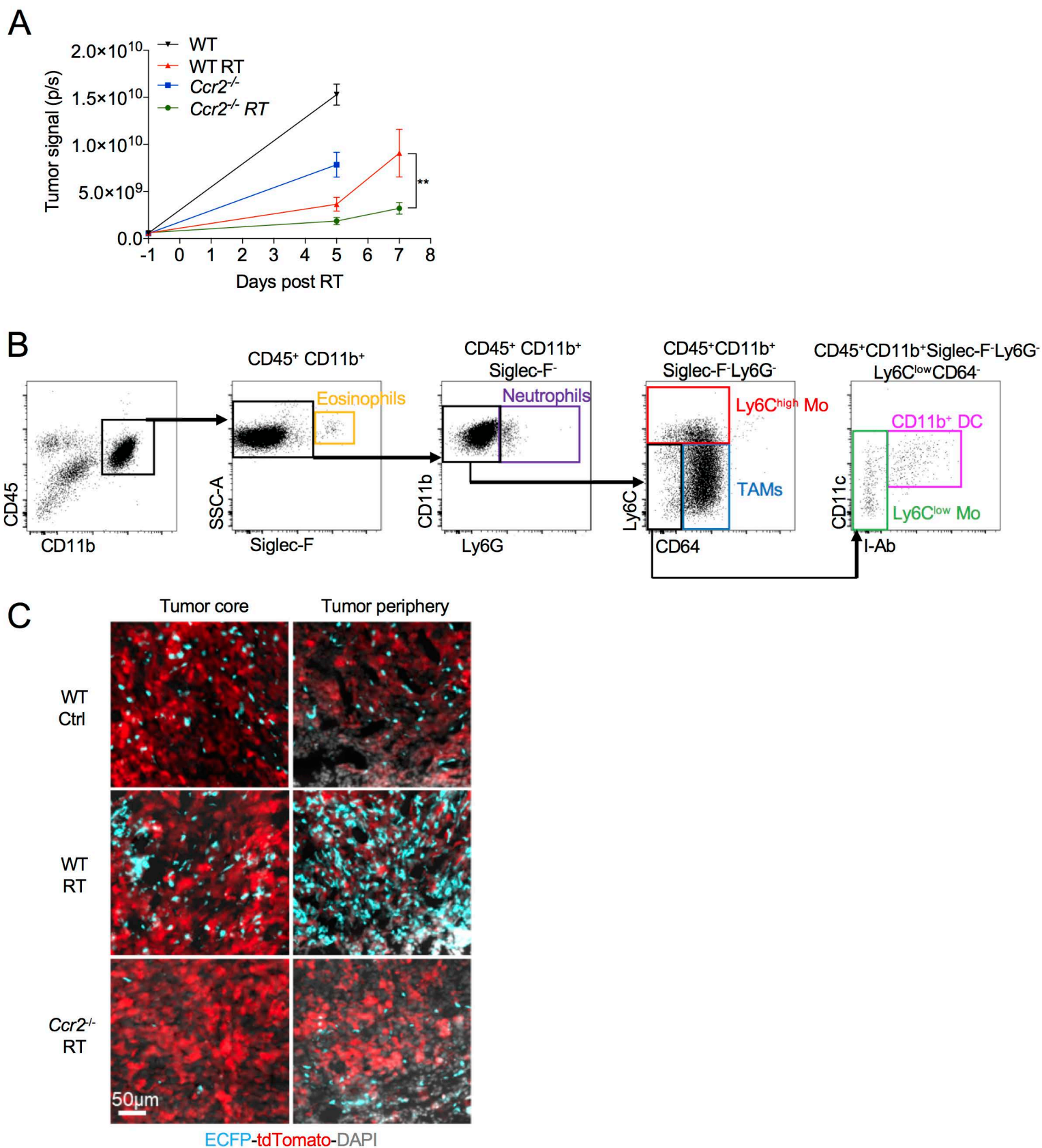


Figure S1

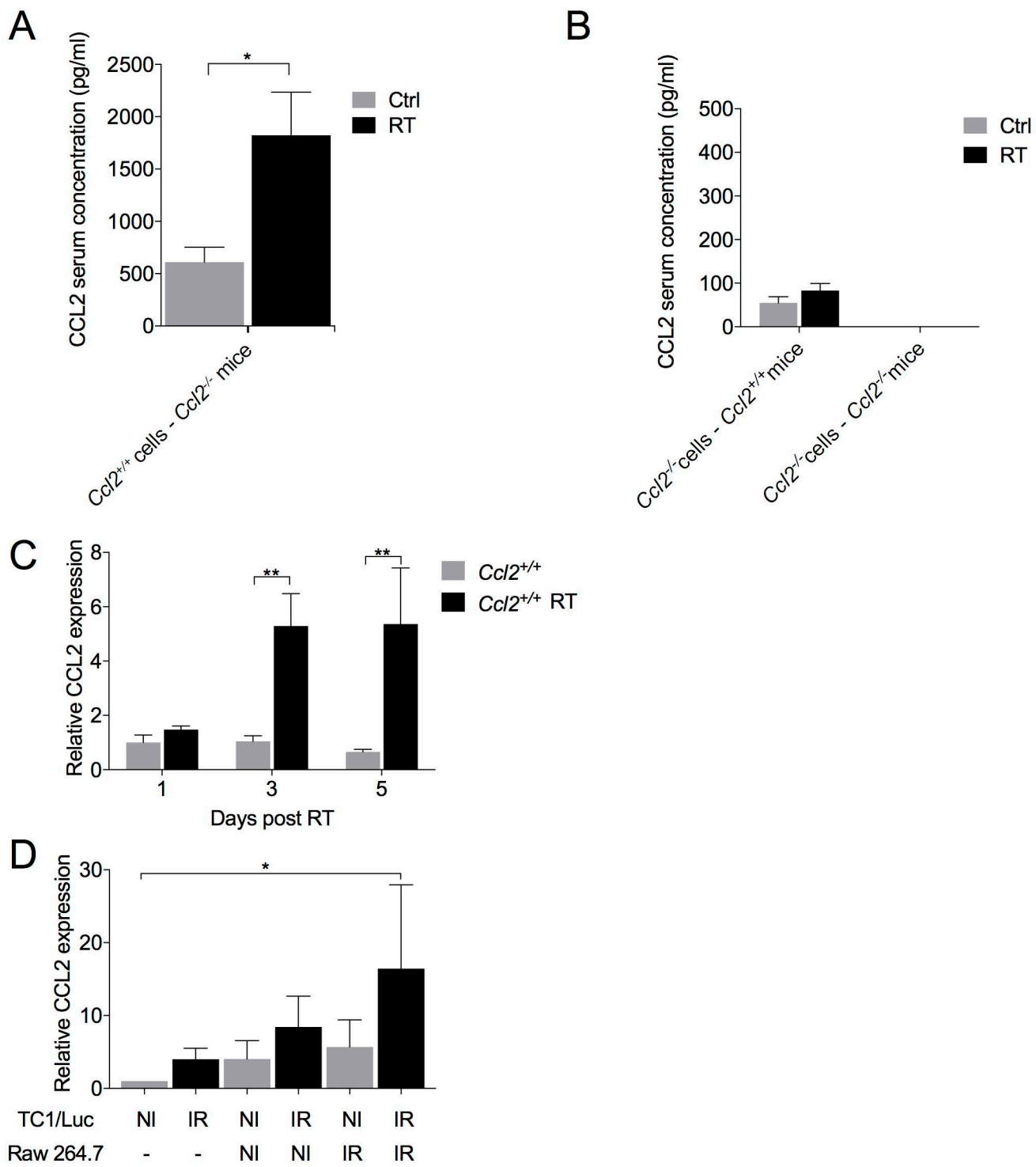


Figure S2

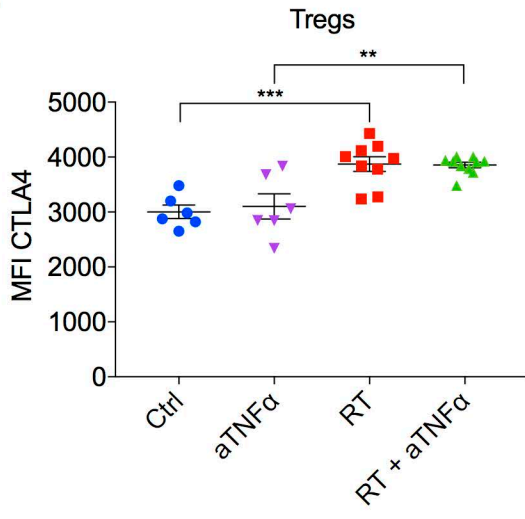
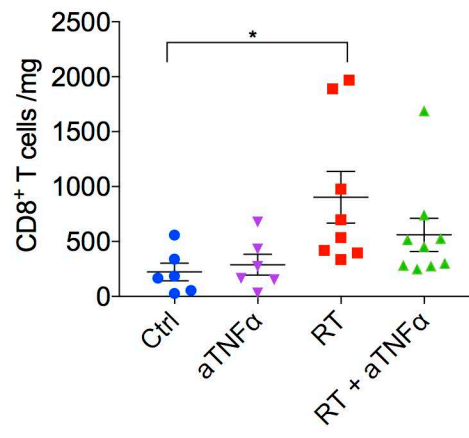
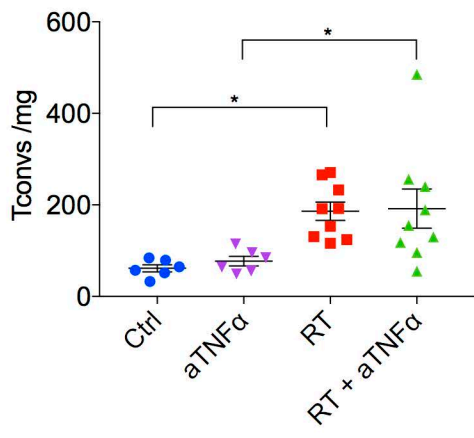
**A****B**

Figure S3

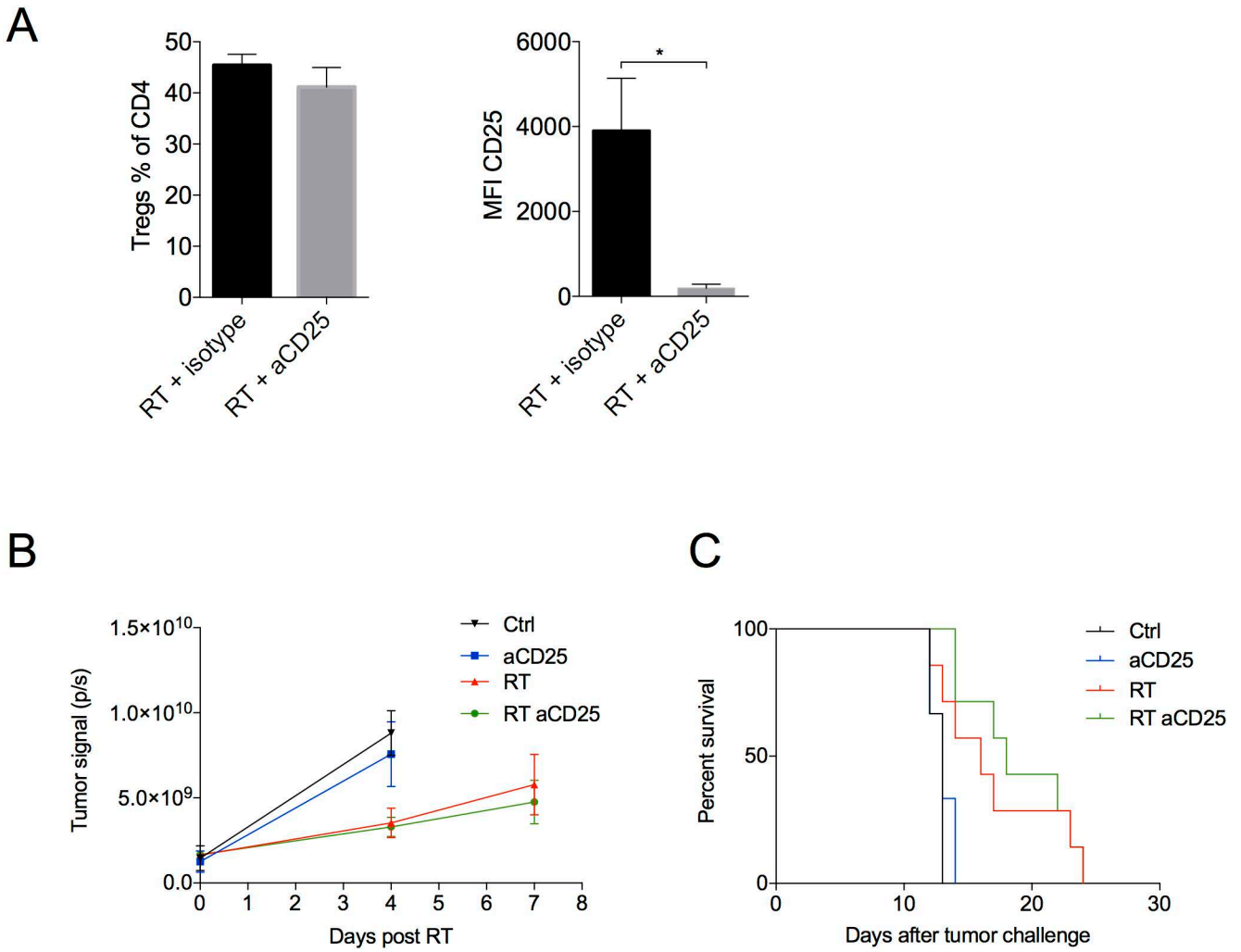


Figure S4